PERGAMON

Atmospheric Environment 36 (2002) 4357–4366

ATMOSPHERIC ENVIRONMENT

www.elsevier.com/locate/atmosenv

A theoretical evaluation on the HNO_3 artifact of the annular denuder system due to evaporation and diffusional deposition of NH_4NO_3-containing aerosols

Kuanfoo Chang[a], Chungsying Lu[a,*], Hsunling Bai[b], Guor-Cheng Fang[c]

[a] *Department of Environmental Engineering, National Chung-Hsing University, Taichung 402, Taiwan*
[b] *Institute of Environmental Engineering, National Chiao-Tung University, 75, Pa-Ai Street, Hsinchu 300, Taiwan*
[c] *Air Toxic and Environmental Analysis Laboratory, Hungkuang Institute of Technology, Sha-Lu, Taichung 433, Taiwan*

Received 7 July 2001; accepted 17 May 2002

Abstract

A mathematical model was developed to evaluate HNO_3 artifact of the annular denuder system due to evaporation and diffusional deposition of nitrate-containing aerosols. The model performance was validated by comparing its numerical solutions with laboratory and numerical data available in the literature for evaporation and diffusional deposition of monodisperse and polydisperse NH_4NO_3 aerosols. Measurement artifacts were evaluated by varying typical sampling ranges of ambient temperature, HNO_3 gas concentration, aerosol number concentration, aerosol mass median diameter, and nitrate mass fraction of $<2.5\,\mu m$ aerosols to see their respective effects. Potential application of the present model on estimating HNO_3 artifacts was demonstrated using literature data sampled in USA, Taiwan, Netherlands, Korea and Japan. Significant measurement artifact could be found in Taiwan and Netherlands due either to low HNO_3 gas concentration and high nitrate concentration in $<2.5\,\mu m$ aerosols or to high ambient temperature.

Keywords: Annular denuder system; Measurement artifact; HNO_3; NH_4NO_3; Evaporation; Mass accommodation coefficient

1. Introduction

The annular denuder system is an instrument being widely employed for sampling and collecting reactive gases such as SO_2, HNO_3, NH_3 and organic vapors in the atmosphere (Koutrakis et al., 1988; Benner et al., 1991; Lee et al., 1993; Matsumoto and Okita, 1998). The sampling mechanism of the denuder is the diffusion of gaseous pollutants onto the denuder walls coated with reactive substances. Despite the fact that the denuder has advantages of allowing high sampling velocities and possessing large sampling capacities, measurement artifacts are possible and may be significant.

As the gaseous pollutants are absorbed onto the denuder wall, the state of equilibrium between the aerosol and gas-phases is disturbed, which may result in evaporation of aerosols and release of additional gaseous pollutants. Therefore, an excessive amount of gaseous pollutants is being sampled. This phenomenon may particularly be true for volatile aerosols such as NH_4NO_3 and NH_4Cl and their associated gases. Furthermore, the diffusional deposition of aerosols containing compounds similar to the sampling gases may also introduce additional gaseous pollutants.

Durham et al. (1987) conducted a study on the nitric acid–nitrate aerosol measurements by a tubular diffusion denuder and compared their experiment data with those predicted by the Gormley–Kennedy equation (Gormley and Kennedy, 1949). The relative errors, which are defined as the difference between measured

*Corresponding author. Fax: +886-4-22862587.
E-mail address: cslu@enve.ev.nchu.edu.tw (C. Lu).

1352-2310/02/$ - see front matter
PII: S1352-2310(02)00352-7

and theoretical results divided by the theoretical result, were in the range of 10–90%. They attributed the deviations to the deposition of gaseous N-compound that is extracted and analyzed as NO_3^- or the released of HNO_3 gas from NH_4NO_3 aerosols during transit in the denuder. Measurement artifacts were found for sampling HNO_3 gas in the study of Bai and Wen (2000). The relative errors strongly depend on the atmospheric HNO_3 concentration and may be as high as over 80%.

Sampling artifacts of the denuder due to evaporation of NH_4NO_3 aerosols have been theoretically studied by Pratsinis et al. (1989) and Biswas et al. (1990). Over 200% excessive absorbed NH_3 gases may occur at 35°C. However, in their studies, the aerosol stream was assumed to contain a monodisperse aerosol. A moment model approximating the aerosol-size distribution by a lognormal function was developed by Bai et al. (1995) to evaluate the evaporation rate of dry NH_4NO_3 and NH_4Cl aerosols. The model was then employed to derive the denuder performance equation for sampling atmospheric HNO_3 gas (Lu et al., 1995). The aerosol polydispersity leads to a significant reduction in the evaporation rate of dry NH_4NO_3 and NH_4Cl aerosols as compared to the monodisperse aerosol. Therefore, the actual measurement artifact may not be as significant as predicted by Pratsinis et al. (1989) and Biswas et al. (1990).

On the other hand, Forrest et al. (1982) and Larson and Taylor (1983) conducted an experiment on the evaporation of NH_4NO_3 aerosols in a tubular diffusion denuder and a parallel-plate stripper, respectively. They concluded that the HNO_3 gas evaporated from NH_4NO_3 aerosols could be neglected as compared to measured HNO_3 gas concentration. Koutrakis et al. (1988) demonstrated the high performance of the Harvard-EPA denuder for sampling atmospheric SO_2, HNO_3 and HNO_2 gases. The differences between measured and calculated collection efficiencies were small in their study. Tsai et al. (2000) found that positive HNO_3 artifact due to volatilization of NH_4NO_3 aerosols is generally negligible compared to measured nitrate-containing particles for an annular denuder and a honeycomb denuder system. According to these studies, the measurement artifacts seem unimportant in a denuder system. However, most of their emphases are on the evaporation of aerosols. Many factors such as ambient temperature, HNO_3 concentration, NH_4NO_3 concentration as well as aerosol size distribution may simultaneously influence the accuracy of HNO_3 measurement.

The mass accommodation coefficient, α, is a kinetics-originating factor describing the interface limitations to the mass transfer between the aerosol and gas-phases. The coefficient is yet not well understood; the process is believed to be inhibited by a resistance in transport of molecules across the particle/air interfaces (Dassios and Pandis, 1999). Bai et al. (1995) used α of 0.1–1 to fit the change of radius of dry NH_4NO_3 aerosol in the denuder. Recently, Dassios and Pandis (1999) found that the α decreases from 0.8 to 0.5 as the temperature increases from 21°C to 27°C. In order to evaluate the effect of organic compounds on the NH_4NO_3 evaporation, Cruz et al. (2000) coated the NH_4NO_3 particles of 100–200 nm diameter with dioctyl phthalate (DOP) and allowed them to evaporate in a constant temperature laminar flow reactor. A decrease, up to 50%, in the evaporation rate of NH_4NO_3 aerosol due to the presence of DOP film was observed which corresponds to the decrease of α from 0.4 to 0.25.

The goals of this study were to develop a mathematical model for identifying atmospheric conditions that may lead to significant HNO_3 artifacts. Major sampling artifacts under consideration are from evaporation and diffusional deposition of NH_4NO_3-containing aerosols. Effects of the two mechanisms on the HNO_3 artifacts for a typical range of atmospheric aerosol and gas properties are evaluated and quantitatively determined.

2. Theory

When NH_4NO_3 aerosols in equilibrium with HNO_3 and NH_3 gases enter the denuder, HNO_3 gas is removed by diffusional absorption at the denuder walls with which the equilibrium is distorted. This results in evaporation of NH_4NO_3 aerosols and release of additional HNO_3 and NH_3 gases.

2.1. Basic assumptions

The following major assumptions are made in developing a mathematical model to study the HNO_3 artifacts in the denuder:

1. The system is in a steady-state operating condition.
2. The flow field in the denuder is a fully developed laminar flow.
3. Only dry atmospheric aerosols are considered, that is, the relative humidity of the atmosphere is below the deliquescent humidity of investigated aerosols.
4. Effect of diffusion in the direction of flow is neglected as compared to convection. This is a valid assumption since the Peclet number of the denuder is much greater than unity.
5. No production or reaction of the gas or aerosol occurs in the denuder.
6. Gas-particle equilibrium, with a modification by introducing α of less than unity, is assumed at the interfaces of solid particles and their surrounding gases and is independent of the denuder residence time.

7. The collection efficiencies of HNO_3 gas and NH_4NO_3-containing aerosols are 100% on the collector wall surface.

2.2. Model development

For NH_4NO_3 aerosols undergoing simultaneous diffusion and evaporation in the denuder, the steady-state general dynamic equation is expressed as (Friedlander, 1977)

$$U_{av}f(r)\frac{\partial n}{\partial z}=\frac{1}{r}\frac{\partial}{\partial r}\left[r\frac{\partial(D_p n)}{\partial r}\right]+\frac{\partial(Gn)}{\partial v}, \tag{1}$$

where U_{av} is the average gas velocity in the denuder, $f(r)$ is the flow profile, r is the radial distance, n is the volume distribution function, z is the axial distance, D_p is the particle diffusivity, G is the volume evaporation/condensation rate ($G<0$ when evaporation is faster than condensation), and v is the volume of an aerosol. The left-hand side (LHS) term accounts for convection of aerosol stream. The first term on the right-hand side (RHS) accounts for radial diffusion of particles. The second RHS term accounts for the loss or gain of particles by evaporation/condensation at rate G. The fully developed flow profile in the denuder is written as (Bird et al., 1960)

$$f(r)=\frac{2[(1-k^2)\ln(r/r_0)+\ln(1/k)(1-r^2/r_0^2)]}{(1+k^2)\ln(1/k)-(1-k^2)}, \tag{2}$$

where k is the inner-to-outer radius ratio, r_0 is the outer radius of the denuder. The G can be expressed as (Friedlander, 1977)

$$G=\frac{dv}{dt}=\frac{2\pi D_m M d_p(p_1-p_d)}{R\rho_p T}\times\left(\frac{1+Kn}{1+0.3773Kn+1.33Kn(1+Kn)/\alpha}\right) \tag{3}$$

where D_m is the diffusivity of NH_4NO_3 monomer, M is the molecule weight, d_p is the particle diameter, p_1 and p_d are the vapor pressures of NH_4NO_3 monomer in the bulk phase and in equilibrium with the aerosol surface, R is the gas constant, ρ_p is the particle density, T is the absolute temperature in K, Kn is the Knudsen number of the particle (Kn is defined as $2\lambda/d_p$, with λ the mean free path of gas molecules).

The evaporation of NH_4NO_3 aerosol leads to the release of HNO_3 and NH_3 gases. The mass balance equation of the gaseous species j is expressed as (Lu et al., 1995)

$$U_{av}f(r)\frac{\partial C_j}{\partial z}=\frac{D_j}{r}\frac{\partial}{\partial r}\left(r\frac{\partial Cj}{\partial r}\right)-\frac{1}{v_m}\int_0^\infty Gn\,dv, \tag{4}$$

where C_j is the concentration of species j (j= HNO_3 or NH_3), D_j is the diffusivity of species j, v_m is the molar volume of NH_4NO_3 aerosol. The LHS term considers convection of species j. The first RHS term considers radial diffusion of species j while the second RHS term considers the gain of species j by aerosol evaporation.

The sectional approach was employed for simulating the evolution of aerosol size distribution along the denuder (Gelbard et al., 1980). The studies of Landgrebe and Pratsinis (1990) showed that the volume-square-based model provided a better prediction on the evolution of aerosol-size distribution than the number-based and volume-based models. Therefore, the volume-square-based model was employed in this study. By dividing the entire aerosol-size domain into L arbitrary sections, the volume-squared size distribution is approximated as follows:

$$Q_I=\int_{v_{I-1}}^{v_I} n(v)v^2\,dv, \tag{5}$$

where Q_I is the aerosol volume-squared concentration in section I ($1\leqslant I\leqslant L$), v_{I-1} and v_I represent the volumes of the smallest and largest aerosols, respectively, in section I.

The governing equations for the sectional volume-squared distribution can be deduced from Eqs. (1) and (4) to give the following partial differential equations (PDEs):

$$\frac{\partial Q_I(r,z)}{\partial z}=\frac{1}{\varepsilon r}\frac{\partial}{\partial r}\left(r\frac{\partial}{\partial r}(\omega Q_I(r,z))\right)+\frac{1}{U_{av}f(r)}(\chi_I Q_I-H_I+H_{I-1}), \tag{6}$$

$$U_{av}f(r)\frac{\partial C_{NH_3}}{\partial z}=\frac{D_{NH_3}}{r}\frac{\partial}{\partial r}\left(r\frac{\partial C_{NH_3}}{\partial r}\right)-(S-1)\zeta\psi\sum_{I=1}^{I=L}\frac{Q_I}{(v_I-v_{I-1})}, \tag{7}$$

$$U_{av}f(r)\frac{\partial C_{HNO_3}}{\partial z}=\frac{D_{HNO_3}}{r}\frac{\partial}{\partial r}\left(r\frac{\partial C_{HNO_3}}{\partial r}\right)-(S-1)\zeta\psi\sum_{I=1}^{I=L}\frac{Q_I}{(v_I-v_{I-1})}, \tag{8}$$

where S is the system saturation ratio (S is defined as $C_{HNO_3}C_{NH_3}/K_P$, with K_P the equilibrium constant of NH_4NO_3 particles with the two associated gases, HNO_3 and NH_3). When the S value is unity, the system is in an external state of equilibrium. The driving force of the evaporation process of NH_4NO_3 particles is determined by $(1-S)$. The definitions of ε, ζ, ω, χ, H_I, H_{I-1}, ζ and ψ are listed in Table 1.

It is assumed that the NH_4NO_3 aerosols and associated gases, HNO_3 and NH_3, reach equilibrium at the denuder inlet ($S=1$ at $z=0$). So the inlet NH_3 concentration can be assumed to be $C_{NH_3,in}=K_p/C_{HNO_3,in}$. The K_p value is taken from Mozurkewich (1993) and can be expressed as

$$\ln K_p=118.87-\frac{24084}{T}-6.025\ln T. \tag{9}$$

Table 1
Definitions of parameters used in the governing equations

χ	$\frac{1}{(v_I - v_{I-1})} \frac{12 D_m M (p_1 - p_d)}{R \rho_p T} \int_{v_{I-1}}^{v_I} \left(\frac{1}{d_p^2} \frac{1 + Kn}{1 + 0.3773 Kn + 1.33 Kn(1 + Kn)/\alpha} \right) dv$
ε	$U_{av} f(r) \int_{v_{I-1}}^{v_I} 1/v^2 \, dv = U_{av} f(r)(1/v_{I-1} - 1/v_I)$
ω	$\int_{v_{I-1}}^{v_I} k_b T C_c / v^2 3\pi\mu d_p \, dv$
φ	$\int_{v_I}^{v_{I+1}} (d_p/v^2)(1 + Kn)/(1 + 0.3773 Kn + 1.33 Kn(1 + Kn)/\alpha) \, dv$
ζ	$(1/v_m)(2\pi D_m p_d M/\rho_p RT)$
H_I	$m_I/(m_{I+1} - m_I)\chi Q_I$
H_{I-1}	$m_{I-1}/(m_I - m_{I-1})\chi_{I-1} Q_{I-1}$

Note: v, volume of an aerosol; D_m, diffusivity of NH_4NO_3 monomer; M, molecular weight; d_p, particle diameter; p_1, bulk phase vapor pressure of NH_4NO_3 monomer; p_d, equilibrium vapor pressure of NH_4NO_3 monomer; R, gas constant; ρ_p, particle density; Kn, Knudsen number; α, accommodation coefficient; U_{av}, average gas velocity; $f(r)$, flow profile; r, radial distance; k_b, Boltzmann's constant; T, ambient temperature; C_c, Cunningham correction factor; μ, dynamic viscosity; v_m, molar volume of NH_4NO_3 aerosol; $m_I = V_I/N_I$; V_I, aerosol volume in section I; N_I, aerosol number in section I; and Q_I, aerosol volume-squared concentration in section I.

The initial condition for the inlet aerosols is

$$Q_I(r, 0) = \int_{I-1}^{I} v^2 n(v, 0) \, dv. \tag{10}$$

The denuder wall is designed as perfect sink for NH_4NO_3 aerosol ($Q_I = 0$) and HNO_3 gas ($C_{HNO_3} = 0$), but inert for NH_3 gas ($C_{NH_3}/\partial r = 0$). The physical quantity of $Q_I = 0$ means the aerosol volume-squared concentration is equal to zero at the denuder wall.

Eq. (6) describes aerosol diffusion and evaporation while Eqs. (7) and (8) consider the diffusion of NH_3 and HNO_3 gases and the source term from evaporation of NH_4HNO_3 aerosol. These equations along with the appropriate boundary conditions constitute a set of coupled PDEs. Using an explicit-finite difference scheme at P radial points across the denuder, the three PDEs are transformed to ordinary differential equations (ODEs). These ODEs are then solved by a stiff ODE solver, DIVPAG (IMSL, 1987). The integrations are solved using the Gauss–Lagendre quadrature method (Hornbeck, 1982). The cup-mixing average is used to evaluate effects of process parameter on the evolution of the aerosol and the gaseous concentrations.

3. Results and discussion

3.1. Numerical stability analysis

Prior to analysis of the denuder performance, the numerical stability of the model is checked. The stability of numerical solutions as a function of grid size ($\Delta r, \Delta z$) and number of sections (L) employed in the model was investigated by a sensitivity analysis. Trials with varying P radial points from 10 to 30, Δz from 10^{-6} to 10^{-4} cm, and L from 5 to 20 were conducted and the results showed that nearly identical solutions are achieved for P radial points $\geqslant 20$, $\Delta z \leqslant 10^{-4}$ and $L \geqslant 10$. Therefore, radial points of 20, Δz of 10^{-4} cm, and L of 10 were used in the following studies.

3.2. Model verification for diffusional deposition of HNO_3 gas and NH_4NO_3 aerosol

The present model for diffusional deposition of HNO_3 gas and NH_4NO_3 aerosol was first examined by comparing its numerical solutions with those predicted by the Gormley–Kennedy equation (Gormley and Kennedy, 1949) in a tubular pipe. The inner-to-outer radius ratio, k, was set to zero and the flow profile is set to $f(r) = 2(1 - r^2/r_0^2)$. The boundary conditions were set to axis of symmetry and zero wall concentration. The aerosol diffusivity was estimated by the Stokes–Einstein expression (Friedlander, 1977) while the diffusivities of NH_3, HNO_3 and NH_4NO_3 monomer were chosen as 0.227, 0.118 (Winiwarter, 1989) and 6.03×10^{-2} cm^2/s (Bai et al., 1995), respectively. The comparison results showed that the numerical solutions predicted by the present model are in excellent agreement with the Gormley–Kennedy solution.

3.3. Model verification for evaporation of a monodisperse NH_4NO_3 aerosol

The present model for evaporation of a monodisperse NH_4NO_3 aerosol was then evaluated by the measured data of Dassios and Pandis (1999). The NH_4NO_3 aerosols of 80–220 nm diameter were evaporated in the reactor under relative humidity of around 10% and temperature of 20–27°C. An average residence time of 30 s was employed in most experiments. The α value is unknown and needs to be justified.

Fig. 1 shows the change in size of the NH_4NO_3 aerosols at 21°C predicted by the present model and measured by Dassios and Pandis (1999). The employed α values were equal to 0.5, 0.8 and 1. As can be seen, close agreement was obtained between the predicted and measured results in the α range of 0.5–1.0. The $\alpha = 0.8$ case provides a best fit to the measured data and was used in the following studies.

3.4. Model verification for evaporation of a polydisperse NH_4NO_3 aerosol

The present model for evaporation of a polydisperse NH_4NO_3 aerosol in the denuder was also tested by the measured data of Harrison et al. (1990). The inlet NH_4NO_3 aerosols were lognormally distributed with a geometric mean radius of 0.46 μm and a standard deviation of 1.6. The temperature and relative humidity were 20 ± 2°C and 30–60%, respectively. The inlet number concentration of NH_4NO_3 aerosol was set to $10^5/cm^3$ (Bai et al., 1995).

Fig. 2 shows the measured and predicted results on the change of particle radius of dry NH_4NO_3 aerosols in the denuder. It is seen that the predicted results agree well with the measured data.

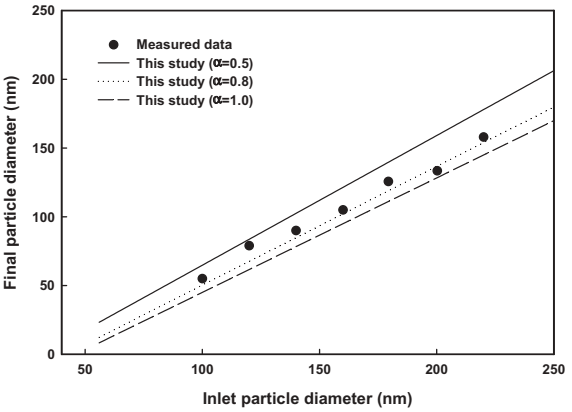

Fig. 1. Comparisons of the change in size for a monodisperse NH_4NO_3 aerosol at 21°C predicted by the present model and measured by Dassios and Pandis (1999).

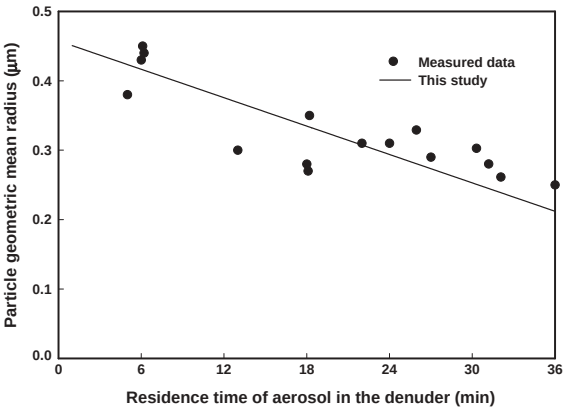

Fig. 2. Comparisons of the change in size for a polydisperse NH_4NO_3 aerosol predicted by the present model and measured by Harrison et al. (1990).

3.5. Model application in the field study

The present model was then applied to predict the measured data of Bai and Wen (2000) for the relative sampling errors of HNO_3 gas by the annular denuder system. Bai and Wen (2000) used three or four denuders in series coated with NaCl for HNO_3 sampling. Assuming that the absorption efficiency of HNO_3 gas (η) is high and the absorption efficiency of the interfering species (η_{int}) is low, the first and second denuders collected both HNO_3 gas and interfering species (C_{HNO_3} and C_{int}) and the third and fourth denuders collected interfering species only; the collected gas concentrations by each denuder are

$$\text{first denuder} = C_{HNO_3}\eta + C_{int}\eta_{int}, \tag{14}$$

$$\text{second denuder} = C_{HNO_3}(1-\eta) + C_{int}\eta_{int}, \tag{15}$$

$$\text{third denuder} = \text{fourth denuder} = C_{int}\eta_{int}. \tag{16}$$

The HNO_3 gas concentration can thus be calculated by subtracting double the concentration collected by the third from the sum of those collected by the first and second denuders. The percentage excess of absorbed HNO_3 gas is calculated as $C_{int}\eta_{int}/C_{HNO_3} \times 100\%$. Detailed information concerning HNO_3 artifact can be seen in Bai and Wen, 2000. Because the size distribution of the atmospheric aerosols was not measured in their study, the atmospheric aerosol and gas properties of the Hsinchu area are adopted from average values of a typical range available in the literature (Lee and Hsu, 1996; Bai and Wen, 1998) and are listed in Table 2.

Fig. 3 shows the predicted and measured results on the percentage excess of absorbed HNO_3 gas in the denuder. As can be seen, the percentage excess of absorbed HNO_3 gas was underpredicted by the present model. This can be attributed to the oxidation of other

Table 2
Typical range of the atmospheric aerosol and gas properties

Parameters	Typical range	Employed values
N_i (#/cm^3)	10^4–10^6	10^5
MMD_i (μm)	0.1–1.0	0.6
M_f (%)	4–12	8
C_i (μg/m^3)	0.2–1.0	0.6

Note: N_i, inlet aerosol number concentration; MMD_i, inlet aerosol mass medium diameter; M_f, nitrate mass fraction of less than 2.5 μm aerosols; and C_i, initial HNO_3 gas concentration.

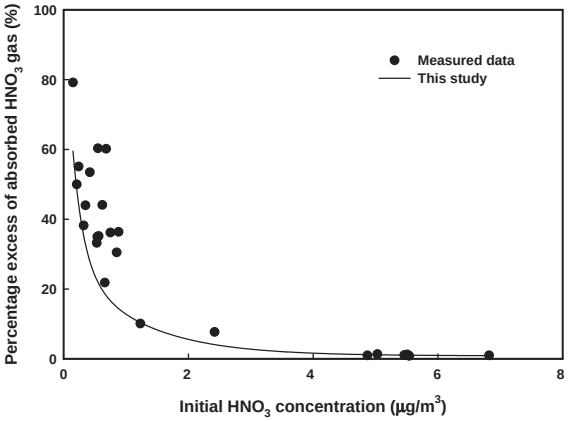

Fig. 3. Comparisons of the percentage excess of absorbed HNO_3 gas predicted by the present model and measured by Bai and Wen (2000).

gaseous N-compounds such as HNO_2 and NO_X to HNO_3 gas, which was not considered in this study. These reactions are still unclear in the literature and further studies are needed to determine the real mechanisms of oxidation and whether they can be controlled. Significant deviations were observed for inlet HNO_3 concentrations $<0.2\,\mu g/m^3$ and could be as high as 40%. However, as the inlet HNO_3 concentrations increased to $1.0\,\mu g/m^3$, the deviations between the measured and predicted results became small. This is because for the same amount of HNO_3 artifact the percentage error is high for low inlet HNO_3 concentration since the denominator in the calculation is low.

3.6. Predicting the excess of absorbed HNO_3 gas

Having established the accuracy and consistency of the present model on the evaporation and diffusional deposition of NH_4NO_3 aerosol in the denuder, a sensitivity analysis of the important parameters on the HNO_3 artifact was carried out. The denuder described in the study of Bai and Wen (2000) was employed. The

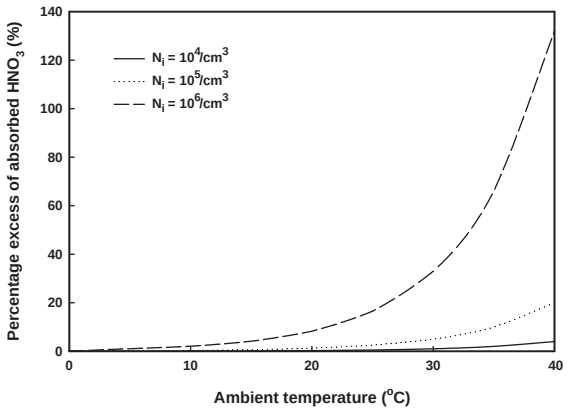

Fig. 4. Predicted percentage excess of absorbed HNO_3 gas as a function of ambient temperature for varying inlet aerosol number concentration (N_i) with inlet conditions of aerosol mass median diameter = 0.6 μm, nitrate mass fraction of <2.5 μm aerosols = 0.08, and inlet HNO_3 gas concentration = 0.6 μg/m^3.

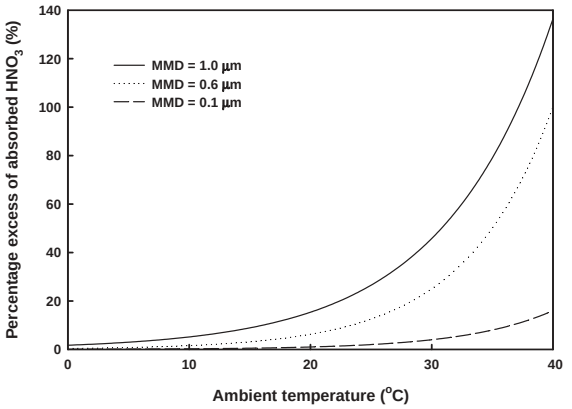

Fig. 5. Predicted percentage excess of absorbed HNO_3 gas as a function of ambient temperature for varying inlet aerosol mass median diameter (MMD_i) with inlet conditions of aerosol number concentration = 10^5/cm^3, nitrate mass fraction of <2.5 μm aerosols = 0.08, and inlet HNO_3 gas concentration = 0.6 μg/m^3.

investigated parameters are: inlet aerosol number concentration (N_i), inlet mass median diameter (MMD_i), nitrate mass fraction of <2.5 μm aerosols (M_f), and inlet HNO_3 gas concentration (C_i). The employed values of Table 2 are selected as the base case. Trials are conducted for each parameter in the high and low levels, keeping all other variables constants as the base case.

Figs. 4–7 show the predicted percentage excess of absorbed HNO_3 as a function of ambient temperature for varying N_i, MMD_i, M_f and C_i, respectively. The residence time of aerosols in the denuder system was set to 1.0 s. The employed ambient temperature was in the range of 15–35°C which is the typical temperature range

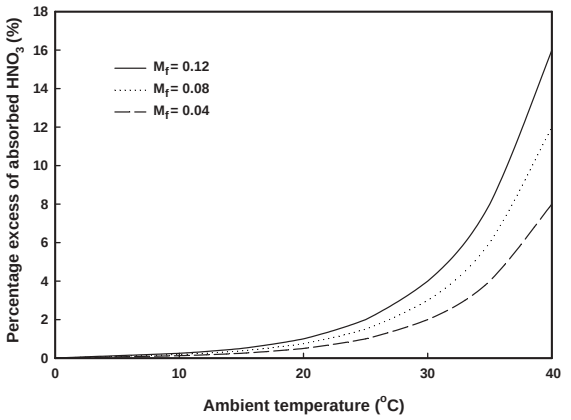

Fig. 6. Predicted percentage excess of absorbed HNO_3 gas as a function of ambient temperature for varying nitrate mass fraction of $<2.5\,\mu m$ aerosols (M_f) with inlet conditions of aerosol mass median diameter $=0.6\,\mu m$, aerosol number concentration $=10^5/cm^3$, and HNO_3 gas concentration $=0.6\,\mu g/m^3$.

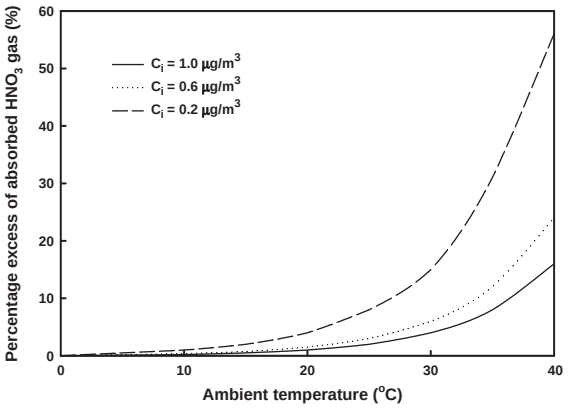

Fig. 7. Predicted percentage excess of absorbed HNO_3 gas as a function of ambient temperature for varying inlet HNO_3 gas concentration (C_i) with inlet conditions of aerosol mass median diameter $=0.6\,\mu m$, aerosol number concentration $=10^5/cm^3$, and nitrate mass fraction of $<2.5\,\mu m$ aerosols $=0.08$.

in Taiwan. It is seen that the percentage excess of absorbed HNO_3 increased as the ambient temperature increased. This can be attributed to the fact that the NH_4NO_3 evaporation rate is dependent on the partial pressure driving force, $p_1 - p_d$ as indicated in Eq. (3). The p_d is a function of ambient temperature. An increase of ambient temperature causes an increase of p_d, and thus results in an increase of partial pressure driving force and NH_4NO_3 evaporation rate.

As can be noted in Fig. 4, the percentage excess of absorbed HNO_3 gas increased as N_i increased. This is due to the fact that an increase of N_i provides a higher NH_4NO_3 mass available for evaporation and release of more HNO_3 gases. Furthermore, more NH_4NO_3-containing aerosols were deposited on the denuder wall for a higher N_i, which may also enhance the HNO_3 artifact. The $N_i = 10^6$ case has a very significant effect on the HNO_3 artifact under ambient temperature $>30^\circ C$. At an ambient temperature of $30^\circ C$, the percentage excess (artifact concentration) of absorbed HNO_3 gas was equal to 33% ($0.2\,\mu g/m^3$), 5% ($0.03\,\mu g/m^3$) and 1% ($0.006\,\mu g/m^3$) for aerosols with N_i of 10^4, 10^5 and $10^6\,cm^{-3}$, respectively.

It is seen in Fig. 5 that a higher sampling artifact is introduced for aerosols with a larger MMD_i. This is due to the fact that for NH_4NO_3-containing aerosols with same M_f and N_i, a larger MMD_i aerosol has a higher NH_4NO_3 mass available for the evaporation and diffusional deposition processes. At an ambient temperature of $30^\circ C$, the percentage excess (artifact concentration) of absorbed HNO_3 gas was equal to 45% ($0.27\,\mu g/m^3$), 20% ($0.12\,\mu g/m^3$) and 2% ($0.012\,\mu g/m^3$) for aerosols with MMD_i of 1.0, 0.6 and $0.1\,\mu m$, respectively.

It is noted in Fig. 6 that the percentage excess of absorbed HNO_3 gas increased as M_f increased. This is again due to a high NH_4NO_3 mass available for evaporation and diffusional deposition processes. However, the effect of M_f on the HNO_3 artifact is relatively small as compared to other parameters. This is because the typical value of M_f in Taiwan was usually <0.1 (Chang et al. 2001). Hence, the M_f was changed only by a factor of three. At an ambient temperature of $30^\circ C$ the percentage excess (artifact concentration) of absorbed HNO_3 gas increased from 2% ($0.012\,\mu g/m^3$) to 4% ($0.024\,\mu g/m^3$) as M_f increased from 0.04 to 0.12.

As can be seen from Fig. 7, an increase of C_i results in a reduction of the percentage excess of absorbed HNO_3 gas increased as C_i decreased, but an opposite trend was observed for artifact concentration. For example, at an ambient temperature of $40^\circ C$ the percentage excess of absorbed HNO_3 gas decreased from 55% to 18% as C_i increased from 0.2 to $1.0\,\mu g/m^3$, respectively, but the artifact concentration increased from 0.11 to $0.18\,\mu g/m^3$. This is because the NH_3–HNO_3–NH_4NO_3 system was assumed to be in equilibrium at the entrance of the denuder. Therefore, the inlet NH_3 gas concentration depends on the inlet HNO_3 gas concentration. For a high inlet HNO_3 gas concentration, the inlet NH_3 gas concentration is low. As the HNO_3 gas is being absorbed rapidly at the denuder wall upon entering the denuder, the evaporation driving force, $S-1$, would be high, which caused a high NH_4NO_3 evaporation rate and thus led to the release of more HNO_3 gas. However, when expressed as the percentage excess of absorbed HNO_3 gas, the artifact becomes relatively low for a high inlet HNO_3 gas concentration since the denominator is high.

Fig. 8 shows the effects of the residence time of aerosols in the denuder from 0 to 5 s on the percentage excess of absorbed HNO_3 gas. With the exception of C_i, the parameter values were adopted from the base case of sensitivity analysis. The C_i was set to 0.1 μg/m^3. As can be seen, the magnitude of HNO_3 artifact was proportional to the residence time of aerosols in the denuder. This is because more HNO_3 gases were evaporated from nitrate-containing aerosols and diffused to the denuder wall at a longer residence time.

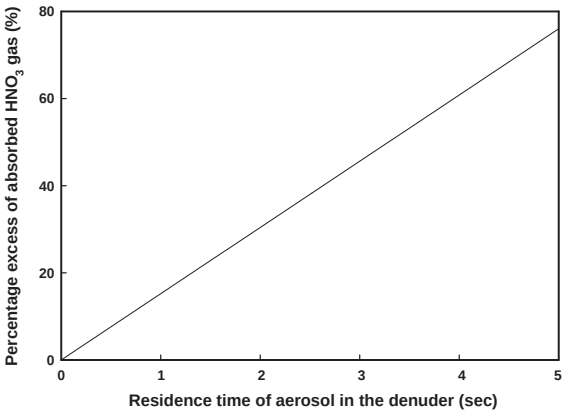

Fig. 8. Predicated percentage excess of absorbed HNO_3 gas as functions of residence time of aerosols in the denuder with inlet conditions of HNO_3 gas concentration = 0.1 μg/m^3, aerosol mass median diameter = 0.6 μm, aerosol number concentration = 10^5/cm^3, nitrate mass fraction of <2.5 μm aerosols = 0.08, and ambient temperature = 30°C.

3.7. Practical application of the present model

Potential application of the present model was demonstrated on estimating the HNO_3 artifact using literature data sampled in USA (Keeler and Spengler, 1991), Taiwan (Perng, 1995), Netherlands (Hoek et al., 1996), Korea (Lee et al., 1997) and Japan (Matsumoto and Okita, 1998) and the results were listed in Table 3. These studies provided the measured data of HNO_3 gas concentration and nitrate concentration in <2.5 μm aerosols. However, the information of aerosol size distribution and ambient temperatures was not available. Therefore, it is assumed that the size distribution of <2.5 μm aerosols was lognormally distributed with N_i of 10^5/cm^3 and MMD_i of 0.6 μm. The HNO_3 artifact was estimated using the highest monthly average temperature in 1 yr. As can be seen in Table 3,

Table 3
Estimated measurement artifacts of HNO_3 gas by one annular denuder for typical gas and aerosol properties available in the literature

Country		Taiwan	USA	Netherlands	Korea	Japan
Reference		Perng (1995)	Keeler and Spengler (1991)	Hoke et al. (1996)	Lee et al. (1997)	Matsumoto and Okita (1998)
Average HNO_3 gas concentration (μg/m^3)		0.30	1.10	0.30	0.80	1.60
[NO_3^-] in less than 2.5 μm aerosols (μg/m^3)	Avg.	10.0	0.4	25.0	2.50	2.24
	Max.	21.6	0.79	51.4	4.53	3.20
The highest monthly average temperature in 1 h[a] (°C)		35	26	27	24	25
Estimated HNO_3 artifact[b] (μg/m^3)	Avg.	0.11	0.0071	0.093	0.017	0.017
	Max.	0.23	0.03	0.22	0.05	0.04
Estimated percentage excess of absorbed HNO_3 (%)	Avg.	35	1.8	31	2.1	1.1
	Max.	77	3.6	73	6.2	2.2

[a] Obtained from http://www.wunderground.com/global/ko.html.
[b] The HNO_3 artifact was estimated using the highest monthly average temperature in 1 yr with the assumption that the size distribution of <2.5 μm aerosols was lognormally distributed with inlet aerosol number concentration of 10^5/cm^3 and aerosol mass medium diameter of 0.6 μm.

significant measurement artifact could be found in Taiwan and Netherlands. This is due either to low HNO_3 gas concentration and high nitrate concentrations in $<2.5\,\mu m$ aerosols or to high ambient temperature. The estimated HNO_3 artifact concentration and the percentage excess of absorbed HNO_3 gas could be as high as $0.23\,\mu g/m^3$ and 77%, respectively. The estimated HNO_3 artifacts for the field data sampled in USA, Korea and Japan were very low as compared to those sampled in Taiwan and Netherlands.

4. Conclusions

A mathematical model was developed to determine the HNO_3 artifact in the denuder due to evaporation and diffusional deposition of NH_4NO_3-containing aerosols. The model performance was validated by comparing its predictions with the measured data for evaporation and diffusional deposition of monodisperse and polydisperse NH_4NO_3 aerosols available in the literature. The neglect of the oxidation of other gaseous N-compounds such as HNO_2 and NO_X to HNO_3 gas may lead to the underprediction of the percentage excess of absorbed HNO_3 gas measured in the field.

The model was then applied to evaluate effects of the important parameters on the HNO_3 artifact. The investigated parameters are: inlet aerosol number concentration (N_i), inlet mass median diameter (MMD_i), nitrate mass fraction of $<2.5\,\mu m$ aerosols (M_f), and inlet HNO_3 gas concentration (C_i). These parameters were usually neglected and unreported in the literature for evaluation of the sampling artifact in the denuder system. For the atmospheric conditions with high values of ambient temperature, N_i, MMD_i and a low value of C_i, the percentage excess of absorbed HNO_3 gas may be significant and therefore should be avoided.

Potential application of the present model on estimating HNO_3 artifact was demonstrated using literature data sampled in USA, Taiwan, Netherlands, Korea and Japan. Significant measurement artifact could be found in Taiwan and Netherlands due either to low HNO_3 gas concentration and high nitrate concentrations in $<2.5\,\mu m$ aerosols or to high ambient temperature.

Ultimately, there are other artifact sources neglected in the present model. Therefore, further experimental and theoretical studies are needed to determine the real mechanisms of the oxidation of other N-compounds to HNO_3 gas in the denuder and whether they can be controlled. The field conditions leading to a significant measurement artifact in the denuder can then be avoided.

Acknowledgements

Support from the National Science Council, Taiwan (NSC89-2211-E-009-058) is gratefully acknowledged.

References

Bai, H., Wen, H.Y., 1998. Applicability of an annular denuder to measure acidic and basic gases in the Hsinchu Area. Journal of the Chinese Institute of Environmental Engineering 8, 73–81.

Bai, H., Wen, H.Y., 2000. Performance of the annular denuder system with different arrangements for HNO_3 and HNO_2 measurements in Taiwan. Journal of the Air and Waste Management Association 50, 125–130.

Bai, H., Lu, C., Ling, Y.M., 1995. A theoretical study on the evaporation of dry ammonium chloride and ammonium nitrate aerosols. Atmospheric Environment 29A, 313–321.

Benner, C.L., Eatough, D.J., Eatough, N.L., Bhardwaja, P., 1991. Comparison of annular denuder system and filter pack collection of $HNO_{3(g)}$, $HNO_{2(g)}$ and particulate-phase nitrate, nitrite and sulfate in the south-west desert. Atmospheric Environment 25A, 1537–1545.

Bird, R.B., Stewart, W.E., Lightfood, E.N., 1960. Transport Phenomena. Wiley, New York.

Biswas, P., Lu, C., Xu, M., Pratsinis, S.E., 1990. Design equations for gas sampling in diffusion denuders and the effect of particle diffusion. In: Mathai, C.V. (Ed.), Transactions on Visibility and Fine Particles, AWMA, Publication No. TR-17, Estes Park, Colorado, USA, October 1989 pp. 131–145.

Chang, K.F., Fang, G.C., Lu, C., Bai, H., 2001. Particle size distribution and anion content at a traffic site in Sha-Lu, Taiwan. Chemosphere 45, 791–799.

Cruz, C.N., Dassios, K.G., Pandis, S.N., 2000. The effect of dioctyl phthalate films on the ammonium nitrate aerosol evaporation rate. Atmospheric Environment 34, 3897–3905.

Dassios, K.G., Pandis, S.N., 1999. The mass accommodation coefficient of ammonium nitrate aerosol. Atmospheric Environment 33, 2993–3003.

Durham, J.L., Spiller, L.L., Ellestad, T.G., 1987. Nitric acid–nitrate aerosol measurements by a diffusion denuder: a performance evaluation. Atmospheric Environment 21, 589–598.

Forrest, J., Spandau, D.J., Tanner, R.L., Newman, L., 1982. Determination of atmospheric nitrate and nitric acid employing a diffusion denuder with a filter pack. Atmospheric Environment 16, 1473–1485.

Friedlander, S.K., 1977. Smoke, Dust and Haze. Wiley, New York.

Gelbard, F., Tambour, Y.R., Seinfeld, J.H., 1980. Sectional representation for simulating aerosols dynamics. Journal of Colloid and Interface Science 76, 541–556.

Gormley, P.G., Kennedy, M., 1949. Diffusion from a stream flowing through a cylindrical tube. Proceedings of the Royal Irish Academic A 52, 163–169.

Harrison, R.M., Sturges, W.T., Kitto, A.N., Li, Y., 1990. Kinetics of evaporation of ammonium chloride and ammonium nitrate aerosols. Atmospheric Environment 24A, 1883–1888.

Hoek, G., Mennen, M.G., Allen, G.A., Hofschreuder, P., Meulen, T.V.D., 1996. Concentrations of acidic air pollutants in the Netherlands. Atmospheric Environment 30 (18), 3141–3150.

Hornbeck, R.W., 1982. Numerical Methods. Prentice-Hall, Englewood Cliffs, NJ.

IMSL (International Mathematics and Statistics Libraries), 1987. Contents Document, Vol. 2. Version 1.0, IMSL, Houston, Texas.

Keeler, G.J., Spengler, J.D., 1991. Acid aerosol measurements at a suburban Connecticut site. Atmospheric Environment 25, 681–690.

Koutrakis, P., Wolfson, J.M., Slater, J.L., Brauer, M., Spengler, J.D., Stevens, R.K., Stone, C.L., 1988. Evaluation of an annular denuder/filter pack system to collect acidic aerosols and glass. Environmental Science and Technology 22, 1463–1468.

Landgrebe, J.D., Pratsinis, S.E., 1990. A discrete-sectional model for particulate production by gas-phase chemical reaction and aerosol coagulation in the free-molecular regime. Journal of Colloid and Interface Science 139, 63–85.

Larson, T.V., Taylor, R.L., 1983. On the evaporation of the ammonium nitrate aerosol. Atmospheric Environment 17, 2489–2495.

Lee, C.T., Hsu, W.C., 1996. The source apportionment of urban aerosols from chemical properties of aerosol spectra near atmospheric sources. Journal of the Chinese Institute of Engineer 19, 1–13.

Lee, H.S., Wadden, R.A., Scheff, P.A., 1993. Measurement and evaluation of acid air pollutants in Chicago using an annular denuder system. Atmospheric Environment 27A, 543–553.

Lee, H.S., Kang, B.W., Cheong, J.P., Lee, S.K., 1997. Relationship between indoor and outdoor air quality during the summer season in Korea. Atmospheric Environment 31 (11), 1689–1693.

Lu, C., Bai, H., Lin, Y.M., 1995. A model for predicting performance of an annular denuder system. Journal of Aerosol Science 26, 1117–1129.

Matsumoto, M., Okita, T., 1998. Long term measurements of atmospheric gaseous and aerosol species using an annular denuder system in Nara, Japan. Atmospheric Environment 32, 1419–1425.

Mozurkewich, M., 1993. The dissociation constant of ammonium nitrate and its dependence on temperature, relative humidity and particle size. Atmospheric Environment 27A, 261–270.

Perng, S.N., 1995. A study of ambient ionic species using diffusion denuder, dichotomous and Hi-Vol PM_{10} samplers. MS Thesis, Institute of Environmental Engineering, National Chiao Tung University, Taiwan.

Pratsinis, S.E., Xu, M., Biswas, P., Willeke, K., 1989. Theory for aerosol sampling through annular diffusion denuders. Journal of Aerosol Science 20, 1597–1600.

Tsai, C.J., Perng, S.B., Chiou, S.F., 2000. Use of two different acidic aerosol samplers to measure acidic aerosols in Hsinchu, Taiwan. Journal of the Air and Waste Management Association 50, 2120–2128.

Winiwarter, W., 1989. A calculation procedure for the determination of the collection efficiency in annular denuder. Atmospheric Environment 23, 1997–2002.